Supporting Information

Theoretical analysis of dynamics of kinesin molecular motors

Ping Xie

Key Laboratory of Soft Matter Physics, Institute of Physics, Chinese Academy of Sciences, Beijing 100190, China

Supporting Text

Analytical studies of dynamics of kinesin molecular motors at non-saturating ATP

S1. Chemomechanical coupling pathway at non-saturating ATP

The chemomechanical coupling pathway of wild-type kinesin dimer at low ATP is schematically shown in Figure S5, similar to that presented before.[S1,S2] We begin the chemomechanical coupling cycle with the trailing head in ATP state binding strongly to site II on an MT filament and the leading head in ADP state binding to site III (Figure S5a). Stimulated by MT, ADP is released from the leading head (Figure S5b). After ATP hydrolysis and Pi release, the trailing head diffuses rapidly to the intermediate position relative to the MT-bound ϕ-head, where the two heads have the high affinity (Figure S5c). After ATP binding to the open nucleotide-binding pocket (NBP) of the MT-bound head (Figure S5d), the subsequent NBP closing and large conformational change of the head take place, weakening greatly its affinity to the ADP-head and inducing its NL docking (see Section S2) (Figure S5e). The detached ADP-head either (with probability P_E) diffuses forward rapidly and binds to the next site IV (Figure S5f) or (with probability $1–P_E$) diffuses backward rapidly and binds to the previous site II (Figure S5g, noting that due to the effect of the NL in the backward and horizontal direction NBP of the leading head becomes open). Stimulated by MT, ADP is released from the trailing head (Figure S5h). After ATP hydrolysis and Pi release in the leading head, the head diffuses rapidly to the intermediate position relative to the MT-bound ϕ-head, where the two heads have the

high affinity (Figure S5i). After ATP binding to the open NBP of the MT-bound head (Figure S5j), the subsequent NBP closing and large conformational change of the head takes place, weakening greatly its affinity to the ADP-head and inducing its NL docking (Figure S5k). The detached ADP-head either (with probability P_E) diffuses forward rapidly and binds to site III (Figure S5a) or (with probability $1–P_E$) diffuses backward rapidly and binds to site I (Figure S5l). Additionally, in Figure S5h before ATP hydrolysis and Pi release occurring in the leading head ATP can also bind to the trailing head (Figure S5m). Similarly, in Figure S5b before ATP hydrolysis and Pi release occurring in the trailing head ATP can also bind to the leading head (Figure S5m). In Figure S5m, if ATP hydrolysis and Pi release take place in the trailing head the system becomes the state of Figure S5d, while if ATP hydrolysis and Pi release take place in the leading head the system becomes the state of Figure S5k.

As shown in Figure 1 (see main text), in Figure S5d and j, ATP hydrolysis and Pi release in the MT-bound head can also take place occasionally before the weakening of the affinity between the two heads takes place, leading to the occurrence of Period I, which is not shown in Figure S5. In Figure S5a or f, ATP hydrolysis and Pi release in the trailing head can also take place occasionally before ADP release from the leading head, leading to the occurrence of Period II, which is also not shown in Figure S5. In Figure S5g or l, ATP hydrolysis and Pi release in the leading head can also take place occasionally before ADP release from the trailing head, also leading to the occurrence of Period II, which is also not shown in Figure S5.

S2. Force-independent but position-dependent ATPase activity and correlations among the ATPase activity, reduction of binding energy between the two heads and NL docking

As defined in the main text, we denote by $k^{(+)}$ the rate of ATP hydrolysis and Pi release of the trailing head, by $k^{(–)}$ the rate of ATP hydrolysis and Pi release of the leading head, with $k^{(+)} >> k^{(–)}$, and by k_D the rate of ADP release from the MT-bound ADP-head. As done before,[S1,S2] we make following definition of rate constants related to ATP binding. ATP can bind to the ϕ-head in any position on MT (whether it is in the leading position or in the INT state or in the trailing position) with a constant second-order binding rate k_b independent of the force. When the head is in the leading position ATP can dissociate with a force-independent rate constant $k_{–1}$, while when the

head is in the trailing position or in the INT state ATP can dissociate with a force-independent rate constant k_{-2} (for simplicity, we take $k_{-2} = 0$, implying that the rate constant of ATP dissociation from the trailing head or the MT-bound head in INT state is very low). The position-dependent ATP-binding efficiency and rate of ATP hydrolysis and Pi release can be understood as follows.

As structural data indicated,[S3] ATP binds firstly to open NBP (with the second-order binding rate k_b), and then NBP can close, which is associated with a large conformational change of the kinesin head. Obviously, ATP has a high rate (k_{-1}) to dissociate from the open NBP, while has a nearly zero rate ($k_{-2} = 0$) to dissociate from the closed NBP. For the leading head, with the NL in the backward and horizontal direction (parallel to the MT filament), due to the NL interference the closing of NBP and large conformational change (or large rotational movement of the central core domain relative to $\alpha 4$ helix bound fixedly to MT) are inhibited. For the trailing head, with the NL in the forward direction, without the NL interference the closing of NBP and large conformational change can occur. For the MT-bound head in INT state, even under the backward load used in optical trapping experiments with micrometer-sized beads the NL of backward direction has an angle more than 45^o with respect to the MT filament,[S4] and thus the NL still does not interfere the closing of NBP and large conformational change. For the open NBP, the rate of ATP hydrolysis and Pi release is very low, with $k^{(-)}$. For the closed NBP, without the effect of the interaction between NL in the forward orientation and head the rate of ATP hydrolysis and Pi release is still very low, with $k^{(-)}$, while the interaction between NL in the forward orientation and head enhances greatly the rate, with $k^{(+)}$. This is consistent with the experimental evidence that the deletion of the NL in the kinesin head reduces greatly its ATPase rate while has no effect on the rate of ADP release,[S5] because after ATP binding and before Pi release the docked NL is in the forward orientation. After Pi release, NBP of the ADP-head becomes open.[S3]

Detailed correlations among the ATPase activity, reduction of binding energy between the two heads and NL docking can be described as follows. After ATP binding, the subsequent closing of NBP and large conformational change of the kinesin head can take place, with a large rotation of $\alpha 6$ helix (to which NL strand $\beta 9$ is connected) relative to $\alpha 4$ helix (which is bound fixedly to MT), as structural data showed.[S6] Then, the NL docking can take place by forming the cover-neck

bundle between $\beta 9$ and motor domain strand $\beta 0$.[S6] The large conformational change of the MT-bound head induced by ATP binding also induces the large reduction of its binding energy with the detached ADP-head, consistent with the atomistic MD simulations.[S7] Thus, both the NL docking under no load and the large reduction of the binding energy between the two heads can take place almost simultaneously, with the rate determined by the conformational change of the head.

S3. Velocity, stepping ratio and dwell time at non-saturating ATP

In the model (Figure S5), probability P_E is independent of ATP concentration. Thus, at non-saturating ATP, P_E can be still calculated by Eq. (4) (see main text). However, it is difficult to derive exactly analytical expressions for the force dependence of quantities such as velocity, stepping ratio, dwell time, etc., at non-saturating ATP. In this section, we provide the approximately analytical expressions.

We begin with its two heads bound simultaneously to MT, with one head in ATP state and the other head in ADP state. There are two states of the dimer. One state (State 1) is that the trailing head is in ATP state and the leading head is in ADP state (Figure S5a), and the other state (State 2) is that the trailing head is in ADP state and the leading head is in ATP state (Figure S5g). During the processive movement of the motor, State 1 occurs with probability P_E, and State 2 occurs with probability $1–P_E$, as noted from Figure S5.

For the case of ATP hydrolysis and Pi release occurring in the trailing head, from State 1 the ATPase rate can be approximately calculated by $\left[1/k^{(+)}+1/\left(k_b[\mathrm{ATP}]\right)\right]^{-1}$. This approximate calculation is under the consideration that at the moment of Pi release occurring in the trailing head ADP has released from the leading head and no ATP is bound to the leading head, because $k_D > k^{(+)}$ and the efficiency of ATP binding to the leading head is low. The approximation is more precise at low ATP concentration while is less precise at the intermediate ATP concentration. From State 2 the ATPase rate can be calculated by $\left[1/k_D+1/\left(k_b[\mathrm{ATP}]\right)+1/k^{(+)}\right]^{-1}$. Thus, for the case of ATP hydrolysis and Pi release occurring in the trailing head, the overall ATPase rate can be approximately calculated by

$$k_{\mathrm{T}} = P_{\mathrm{E}}\left(\frac{1}{k^{(+)}} + \frac{1}{k_{\mathrm{b}}[\mathrm{ATP}]}\right)^{-1} + \left(1 - P_{\mathrm{E}}\right)\left(\frac{1}{k_{\mathrm{D}}} + \frac{1}{k_{\mathrm{b}}[\mathrm{ATP}]} + \frac{1}{k^{(+)}}\right)^{-1}. \quad \text{(S1)}$$

Note that at saturating ATP, Eq. (S1) is reduced to Eq. (1).

For the case of ATP hydrolysis and Pi release occurring in the leading head, from State 1 the ATPase rate can be calculated by $\left[1/k_{\mathrm{D}} + 1/\left(k_{\mathrm{b}}[\mathrm{ATP}]\right) + 1/k^{(-)} + k_{-1}/\left(k_{\mathrm{b}}[\mathrm{ATP}]k^{(-)}\right)\right]^{-1}$. Considering that before hydrolysis ATP can dissociate from the leading head, from State 2, the ATPase rate can be approximately calculated by $\left[1/k^{(-)} + 1/\left(k_{\mathrm{b}}[\mathrm{ATP}]\right) + k_{-1}/\left(k_{\mathrm{b}}[\mathrm{ATP}]k^{(-)}\right)\right]^{-1}$. This approximate calculation is under the consideration that at the moment of Pi release occurring in the leading head ADP has released from the trailing head and ATP has bound to the trailing head, because $k_{\mathrm{D}} >> k^{(-)}$ and the ATP-binding efficiency to the trailing head is much higher than that to the leading head. Thus, for the case of ATP hydrolysis and Pi release occurring in the leading head, the overall ATPase rate can be approximately calculated by

$$k_{\mathrm{L}} = P_{\mathrm{E}}\left(\frac{1}{k_{\mathrm{D}}} + \frac{1}{k_{\mathrm{b}}[\mathrm{ATP}]} + \frac{1}{k^{(-)}} + \frac{k_{-1}}{k_{\mathrm{b}}[\mathrm{ATP}]k^{(-)}}\right)^{-1} + \left(1 - P_{\mathrm{E}}\right)\left(\frac{1}{k^{(-)}} + \frac{1}{k_{\mathrm{b}}[\mathrm{ATP}]} + \frac{k_{-1}}{k_{\mathrm{b}}[\mathrm{ATP}]k^{(-)}}\right)^{-1}. \quad \text{(S2)}$$

Note that at saturating ATP, Eq. (S2) is reduced to Eq. (2).

Consequently, the overall ATPase rate of the dimer can be calculated by

$$k = k_{\mathrm{T}} + k_{\mathrm{L}}. \quad \text{(S3)}$$

The overall forward stepping rate of the motor is $P_{\mathrm{E}}k_{\mathrm{T}}$, backward stepping rate is $(1–P_{\mathrm{E}})k_{\mathrm{L}}$, and ATPase rate with no stepping is $\omega_0 = (1–P_{\mathrm{E}})k_{\mathrm{T}} + P_{\mathrm{E}}k_{\mathrm{L}}$. The stepping ratio can be calculated by

$$r = \frac{P_{\mathrm{E}}k_{\mathrm{T}}}{\left(1 - P_{\mathrm{E}}\right)k_{\mathrm{L}}}. \quad \text{(S4)}$$

The velocity can be calculated by

$$v = \left[P_{\mathrm{E}}k_{\mathrm{T}} - \left(1 - P_{\mathrm{E}}\right)k_{\mathrm{L}}\right]d, \quad \text{(S5)}$$

where d = 8.2 nm. The dwell time between two mechanical steps can be calculated by

$$T_{\mathrm{d}} = \frac{1}{P_{\mathrm{E}}k_{\mathrm{T}} + \left(1 - P_{\mathrm{E}}\right)k_{\mathrm{L}}}. \quad \text{(S6)}$$

Here, we compare the theoretical results obtained using Eqs. (S1) – (S6) with the single molecule data for *Drosophila* kinesin measured by Carter and Cross[S8] and for

bovine brain kinesin measured by Nishiyama et al.[S9] First, we focus on bovine brain kinesin. We take $k^{(+)} = 136\ \ \mathrm{s}^{-1}$, $k^{(-)} = 4\ \ \mathrm{s}^{-1}$, $E_{\mathrm{NL}} = 2.1k_{\mathrm{B}}T$, $d^{(+)} = 3$ nm, $k_{\mathrm{D}} = 250\ \ \mathrm{s}^{-1}$, $k_{\mathrm{b}} = 5\ \ \mu\mathrm{M}^{-1}\mathrm{s}^{-1}$ and $k_{-1} = 100\ \ \mathrm{s}^{-1}$ in calculations (see Table S1). The theoretical results (lines) and experimental results by Nishiyama et al.[S9] (symbols) of velocity, stepping ratio and dwell time versus force at [ATP] = 10 μM and 1 mM are shown in Figure S6a – c (left panels of Figure S6). It is seen that the theoretical and experimental results are in agreement with each other. Then, we focus on *Drosophila* kinesin. As shown in the main text, under the experimental conditions of Carter and Cross[S8] the parameter values are the same as those given in Table 1 except $d^{(+)} = 3.8$ nm (see Table S1). In addition, we take $k_{\mathrm{b}} = 2\ \ \mu\mathrm{M}^{-1}\mathrm{s}^{-1}$ and $k_{-1} = 80\ \ \mathrm{s}^{-1}$ (see Table S1). The theoretical results (lines) and experimental results by Carter and Cross[S8] (symbols) of velocity, stepping ratio and dwell time versus force at [ATP] = 10 μM and 1 mM are shown in Figure S6d – f (right panels of Figure S6). It is seen that the theoretical and experimental results are also in agreement with each other.

S4. Velocity, stepping ratio and dwell time under $k_{\mathrm{D}} >> k^{(+)} >> k^{(-)}$

Since for kinesin-1 ADP release is a non-rate limiting step of the ATPase activity, it is interesting to simplify Eqs. (S1) – (S6) under $k_{\mathrm{D}} >> k^{(+)} >> k^{(-)}$. In the limit of $k_{\mathrm{D}} \to \infty$, Eqs. (S1) and (S2) become

$$k_{\mathrm{T}} = \left(\frac{1}{k^{(+)}} + \frac{1}{k_{\mathrm{b}}[\mathrm{ATP}]} \right)^{-1} = \frac{k^{(+)}[\mathrm{ATP}]}{k^{(+)}/k_{\mathrm{b}} + [\mathrm{ATP}]}, \tag{S7}$$

$$k_{\mathrm{L}} = \left(\frac{1}{k^{(-)}} + \frac{1}{k_{\mathrm{b}}[\mathrm{ATP}]} + \frac{k_{-1}}{k_{\mathrm{b}}[\mathrm{ATP}]k^{(-)}} \right)^{-1} = \frac{k^{(-)}[\mathrm{ATP}]}{\left(k^{(-)} + k_{-1}\right)/k_{\mathrm{b}} + [\mathrm{ATP}]}. \tag{S8}$$

It is seen that k_{T} and k_{L} are now independent of the force F.

Substituting Eq. (4) for probability P_{E} (see main text) and Eqs. (S7) and (S8) into Eq. (S4), we have

$$r = r_0 \exp\left(-\beta F d^{(+)}\right), \tag{S9}$$

$$r_0 = \frac{k^{(+)}}{k^{(-)}} \frac{\left(k^{(-)} + k_{-1}\right)/k_{\mathrm{b}} + [\mathrm{ATP}]}{k^{(+)}/k_{\mathrm{b}} + [\mathrm{ATP}]} \exp\left(\beta E_{\mathrm{NL}}\right). \tag{S10}$$

It is seen that r is an exponential function of F, with r_0 being dependent on [ATP] and the slop of $\ln(r)$ versus F being independent of F. Eqs. (S9) and (S10) can be

rewritten as

$$r = r_0^{(1-F/F_S)}, \tag{S11}$$

$$F_S = \frac{1}{\beta d^{(+)}} \ln\left[\frac{k^{(+)}}{k^{(-)}} \frac{\left(k^{(-)} + k_{-1}\right)/k_b + [\mathrm{ATP}]}{k^{(+)}/k_b + [\mathrm{ATP}]}\right] + \frac{E_{NL}}{d^{(+)}}. \tag{S12}$$

From Eq. (S12) it is seen that if value of $k^{(-)} + k_{-1}$ is evidently different from that of $k^{(+)}$ the stall force is dependent sensitively on [ATP], explaining the single molecule data for squid optic lobe kinesin measured by Visscher et al.[S10] However, if value of $k^{(-)} + k_{-1}$ is close to that of $k^{(+)}$ the stall force is insensitive to [ATP], explaining the single molecule data for bovine brain kinesin measured by Nishiyama et al.[S9] and for *Drosophila* kinesin measured by Carter and Cross[S8] (see Figure S6).

With Eqs. (S9) – (S12), Eq. (4) for probability P_E can be rewritten as

$$P_E = \frac{r_0^{(1-F/F_S)}}{r_0^{(1-F/F_S)} + \frac{k^{(+)}}{k^{(-)}} \frac{\left(k^{(-)} + k_{-1}\right)/k_b + [\mathrm{ATP}]}{k^{(+)}/k_b + [\mathrm{ATP}]}}. \tag{S13}$$

Substituting Eqs. (S7), (S8) and (S13) into Eq. (S5), we have

$$v = \frac{r_0^{(1-F/F_S)} - 1}{r_0^{(1-F/F_S)} + \frac{k^{(+)}}{k^{(-)}} \frac{\left(k^{(-)} + k_{-1}\right)/k_b + [\mathrm{ATP}]}{k^{(+)}/k_b + [\mathrm{ATP}]}} \frac{k^{(+)}[\mathrm{ATP}]}{k^{(+)}/k_b + [\mathrm{ATP}]} d. \tag{S14}$$

Substituting Eqs. (S7), (S8) and (S13) into Eq. (S6), we have

$$T_d = \frac{r_0^{(1-F/F_S)} + \frac{k^{(+)}}{k^{(-)}} \frac{\left(k^{(-)} + k_{-1}\right)/k_b + [\mathrm{ATP}]}{k^{(+)}/k_b + [\mathrm{ATP}]}}{r_0^{(1-F/F_S)} + 1} \frac{k^{(+)}/k_b + [\mathrm{ATP}]}{k^{(+)}[\mathrm{ATP}]}. \tag{S15}$$

S5. Velocity, stepping ratio and dwell time at saturating ATP

At saturating ATP, Eqs. (S1) and (S2) become

$$k_T = P_E k^{(+)} + (1 - P_E) \frac{k_D k^{(+)}}{k_D + k^{(+)}}, \tag{S16}$$

$$k_L = P_E \frac{k_D k^{(-)}}{k_D + k^{(-)}} + (1 - P_E) k^{(-)}. \tag{S17}$$

Eqs. (S16) and (S17) are identical to Eqs. (1) and (2), respectively.

In the limit of $k_D \to \infty$, Eqs. (S16) and (S17) become

$$k_T = k^{(+)}, \tag{S18}$$

$$k_{\mathrm{L}} = k^{(-)}, \tag{S19}$$

Eqs. (S11) and (S12) become

$$r = r_0^{(1-F/F_{\mathrm{S}})}, \tag{S20}$$

$$F_{\mathrm{S}} = \frac{1}{\beta d^{(+)}} \ln\left(\frac{k^{(+)}}{k^{(-)}}\right) + \frac{E_{\mathrm{NL}}}{d^{(+)}}, \tag{S21}$$

Eq. (S14) becomes

$$v = \frac{r_0^{(1-F/F_{\mathrm{S}})} - 1}{r_0^{(1-F/F_{\mathrm{S}})} + \dfrac{k^{(+)}}{k^{(-)}}} k^{(+)} d, \tag{S22}$$

and Eq. (S15) becomes

$$T_{\mathrm{d}} = \frac{r_0^{(1-F/F_{\mathrm{s}})} + \dfrac{k^{(+)}}{k^{(-)}}}{r_0^{(1-F/F_{\mathrm{s}})} + 1} \frac{1}{k^{(+)}}. \tag{S23}$$

As expected, Eqs. (S20) – (S23) are identical to those derived before.[S1,S2]

S6. Run length at non-saturating ATP

First, we do not consider the dissociation in the strong MT-binding state. Based on the model, at non-saturating ATP the dissociation rate can be approximately calculated by

$$\varepsilon_{\mathrm{w}} = kP_{\mathrm{I}} + kP_{\mathrm{II}}P_{d\mathrm{II}}, \tag{S24}$$

where k is calculated by Eqs. (S1) – (S3), which are dependent on ATP concentration, while P_{I}, P_{II} and P_{dII} are calculated by Eqs. (13), (14), (16), (18) and (19) (see main text), which are independent of ATP concentration. It is noted here that at low ATP, Period I can occur after ATP hydrolysis and Pi release in the leading head, because the trailing head is usually in ϕ state with undocked NL. The run length can then be calculated by

$$L = \frac{v}{\varepsilon_{\mathrm{w}}}. \tag{S25}$$

With parameter values given in Table 1 for *Drosophila* kinesin, the theoretical results of run length versus ATP concentration for different values of F calculated by using Eqs. (S1) – (S3), (S5), (S24) and (S25) are shown in Figure S7 (dashed lines). As expected, the run length is nearly independent of ATP concentration. This is understandable. Since P_{I}, P_{II} and P_{dII} are independent of ATP concentration, each

ATPase cycle has a nearly constant dissociation probability if dissociation can only occur in the weak MT-binding state. Thus, it is expected that for any ATP concentration, the motor will takes nearly constant number of steps before dissociation and thus the motor has a nearly constant run length.

Then, we consider the dissociations in both the weak and strong MT-binding states. At non-saturating ATP the dissociation rate can still be calculated by

$$\varepsilon = \varepsilon_{\mathrm{w}} + \varepsilon_{\mathrm{s}}, \tag{S26}$$

where ε_{s} is calculated by Eq. (22) (see main text), which is independent of ATP concentration. The run length can then be calculated by

$$L = \frac{v}{\varepsilon}. \tag{S27}$$

From Eqs. (S26) and (S27) it is noted that the dependence of run length on ATP concentration arises almost solely from the dissociation in the strong MT-binding state. Since under a constant *F* velocity *v* decreases with the decrease of [ATP] and ε_{s} has a constant value independent of [ATP], it is expected that the run length will decrease with the decrease of [ATP]. For the case of $\varepsilon_{\mathrm{w}} >> \varepsilon_{\mathrm{s}}$, e.g., under a low forward force (see Figures 3d and 4d in main text), the change of ATP concentration will have only a slight effect on the run length, which is consistent with the single molecule data of Andreasson et al.[S11] By contrast, for the case of ε_{w} comparable to or smaller than ε_{s}, e.g., under no or a backward force (see Figures 3d and 4d in main text), the change of ATP concentration will have a large effect on the run length, which is consistent with the single molecule data of Schnitzer et al.[S12] For example, with parameter values given in Table S1 for *Drosophila* kinesin and taking $\varepsilon_{\mathrm{s0}} = 0.01$ s^{-1} (as mentioned in the main text, with $\varepsilon_{\mathrm{s0}}$ the other parameter δ_{s} can be determined), the theoretical results of run length versus ATP concentration for different values of *F* calculated by using Eqs. (S1) – (S3), (S5) and (S24) – (S27) are shown in Figure S7 (solid lines). With parameter values given in Table 1 for squid optic lobe kinesin and taking $k_{\mathrm{b}} = 2$ $\mu\mathrm{M}^{-1}\mathrm{s}^{-1}$, $k_{-1} = 10$ s^{-1} and $\varepsilon_{\mathrm{s0}} = 0.02$ s^{-1}, the theoretical results of run length versus ATP concentration for different values of *F* are consistent with the single molecule data of Schnitzer et al.[S12] (Figure S8).

Supporting figures

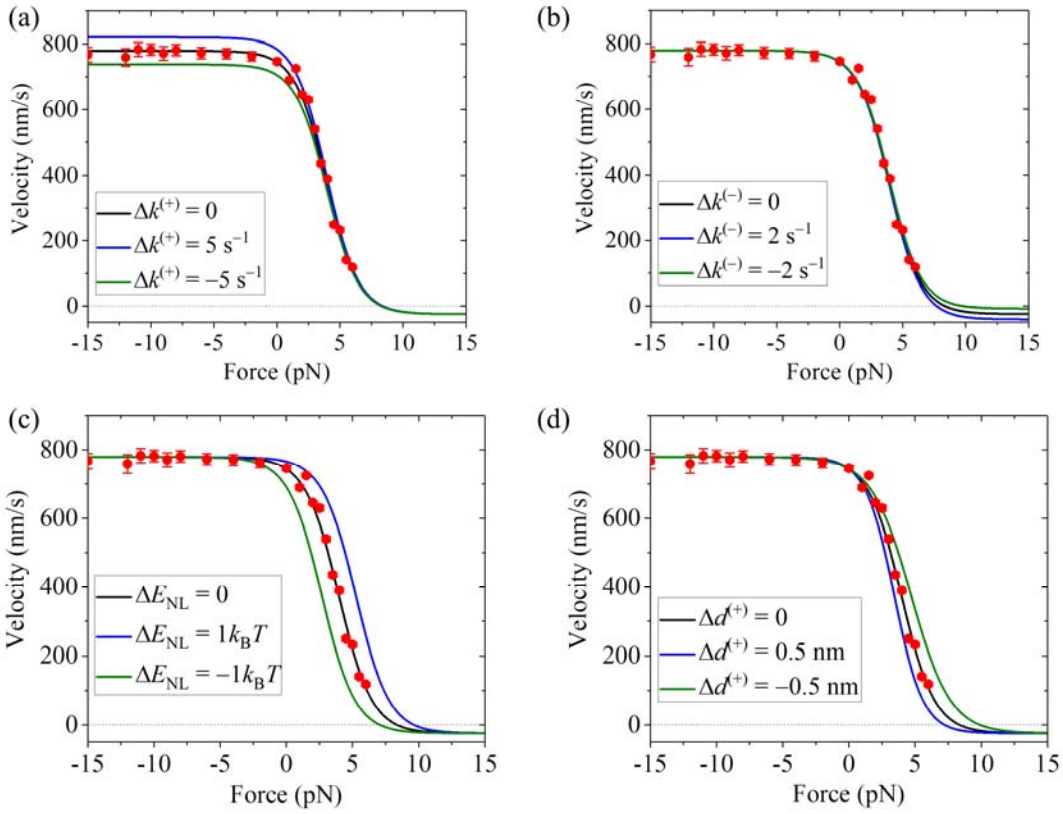

Figure S1. Effects of variation in the individual fitting parameters on results of velocity versus force for *Drosophila* kinesin. Lines are theoretical results calculated using Eq. (10) and with $k^{(+)} = 95\ \ s^{-1}$, $k^{(-)} = 3\ \ s^{-1}$, $E_{NL} = 3.34k_BT$ and $d^{(+)} = 3.5$ nm (see main text) unless otherwise indicated. Symbols are experimental data taken from Andreasson et al.[S11] **(a)** Variation of $k^{(+)}$ by $\Delta k^{(+)}$. **(b)** Variation of $k^{(-)}$ by $\Delta k^{(-)}$. **(c)** Variation of E_{NL} by ΔE_{NL}. **(d)** Variation of $d^{(+)}$ by $\Delta d^{(+)}$.

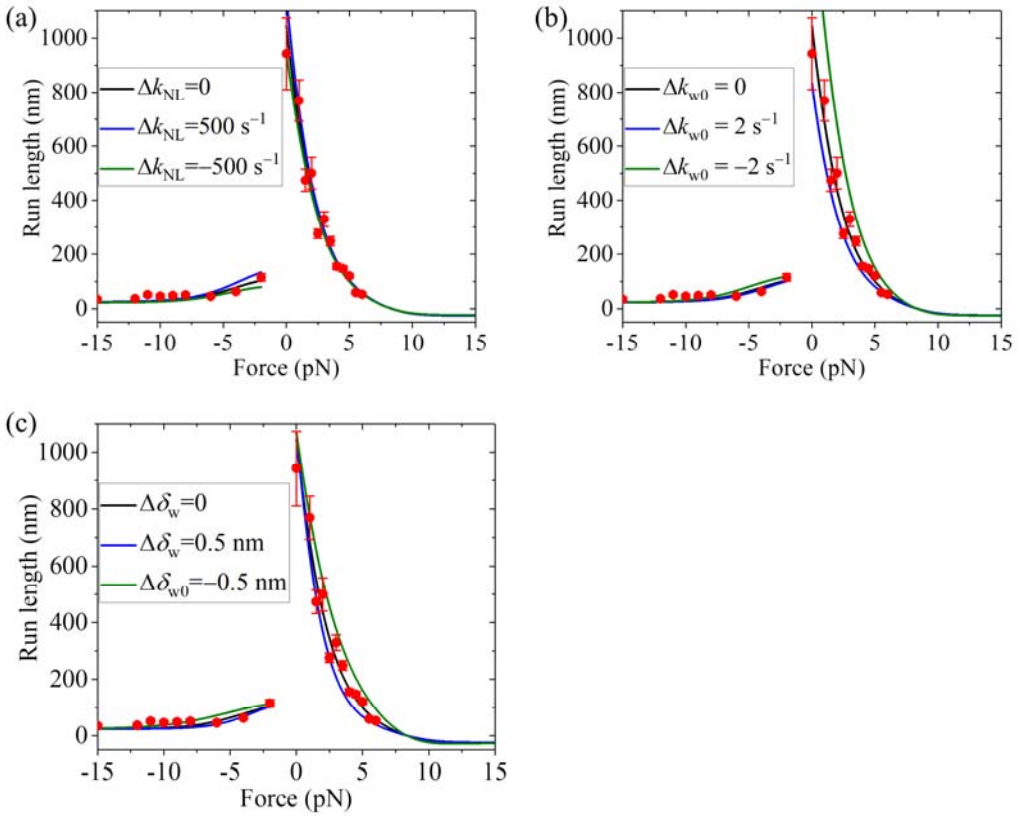

Figure S2. Effects of variation in the individual fitting parameters on results of run length versus force for *Drosophila* kinesin when dissociation only in the weak MT-binding state is considered. Lines are theoretical results calculated with parameter values given in Table 1 for *Drosophila* kinesin (with k_{NL} = 1500 s^{-1}, k_{w0} = 5 s^{-1} and δ_w = 2.2 nm) unless otherwise indicated. Symbols are experimental data taken from Andreasson et al.[S11] **(a)** Variation of k_{NL} by Δk_{NL}. **(b)** Variation of k_{w0} by Δk_{w0}. **(c)** Variation of δ_w by $\Delta\delta_w$.

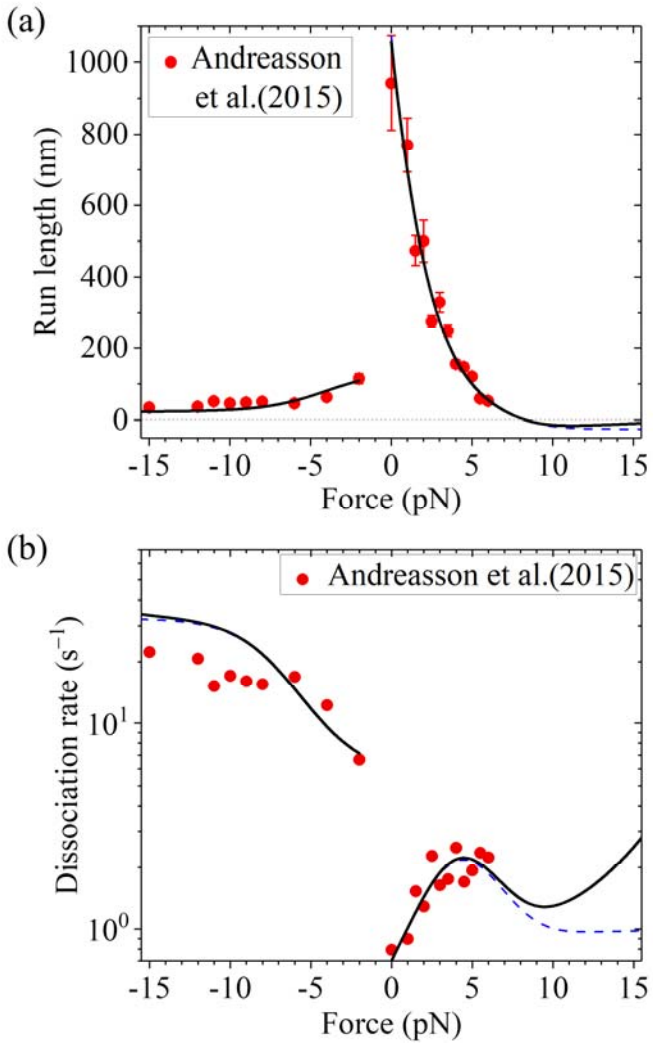

Figure S3. Results for *Drosophila* kinesin motor at saturating ATP. Lines are theoretical results, and symbols are experimental data taken from Andreasson et al.[S11] **(a)** Run length versus external force. The dashed blue line represents the theoretical results calculated by considering that the motor can only dissociate in the weak MT-binding state, and the black solid line represents the theoretical results calculated by considering that the motor can dissociate in both the weak and strong MT-binding states, with $\varepsilon_{s0} = 0.01\ \text{s}^{-1}$. Since the dashed blue line is almost coincident with the black solid line at $F < -2$ pN, the two lines at $F < -2$ pN are almost indistinguishable. **(b)** Dissociation rate versus external force. The dashed blue line represents the theoretical results calculated by considering that the motor can only dissociate in the weak MT-binding state, and the black solid line represents the theoretical results calculated by considering that the motor can dissociate in both the weak and strong MT-binding states, with $\varepsilon_{s0} = 0.01\ \text{s}^{-1}$.

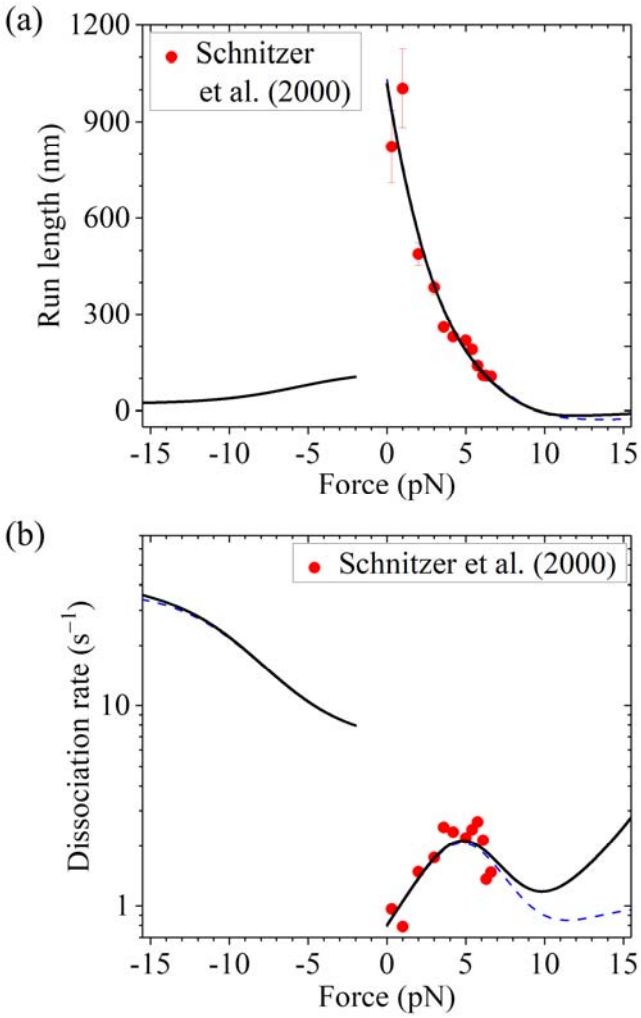

Figure S4. Results for squid optic lobe kinesin motor at saturating ATP. Lines are theoretical results, and symbols are experimental data taken from Schnitzer et al.[S12] (adapted by permission from Springer Nature). **(a)** Run length versus external force. The dashed blue line represents the theoretical results calculated by considering that the motor can only dissociate in the weak MT-binding state, and the black solid line represents the theoretical results calculated by considering that the motor can dissociate in both the weak and strong MT-binding states, with $\varepsilon_{s0} = 0.01\ \text{s}^{-1}$. Since the dashed blue line is almost coincident with the black solid line at $F < -2$ pN, the two lines at $F < -2$ pN are almost indistinguishable. **(b)** Dissociation rate versus external force. The dashed blue line represents the theoretical results calculated by considering that the motor can only dissociate in the weak MT-binding state, and the black solid line represents the theoretical results calculated by considering that the motor can dissociate in both the weak and strong MT-binding states, with $\varepsilon_{s0} = 0.01\ \text{s}^{-1}$.

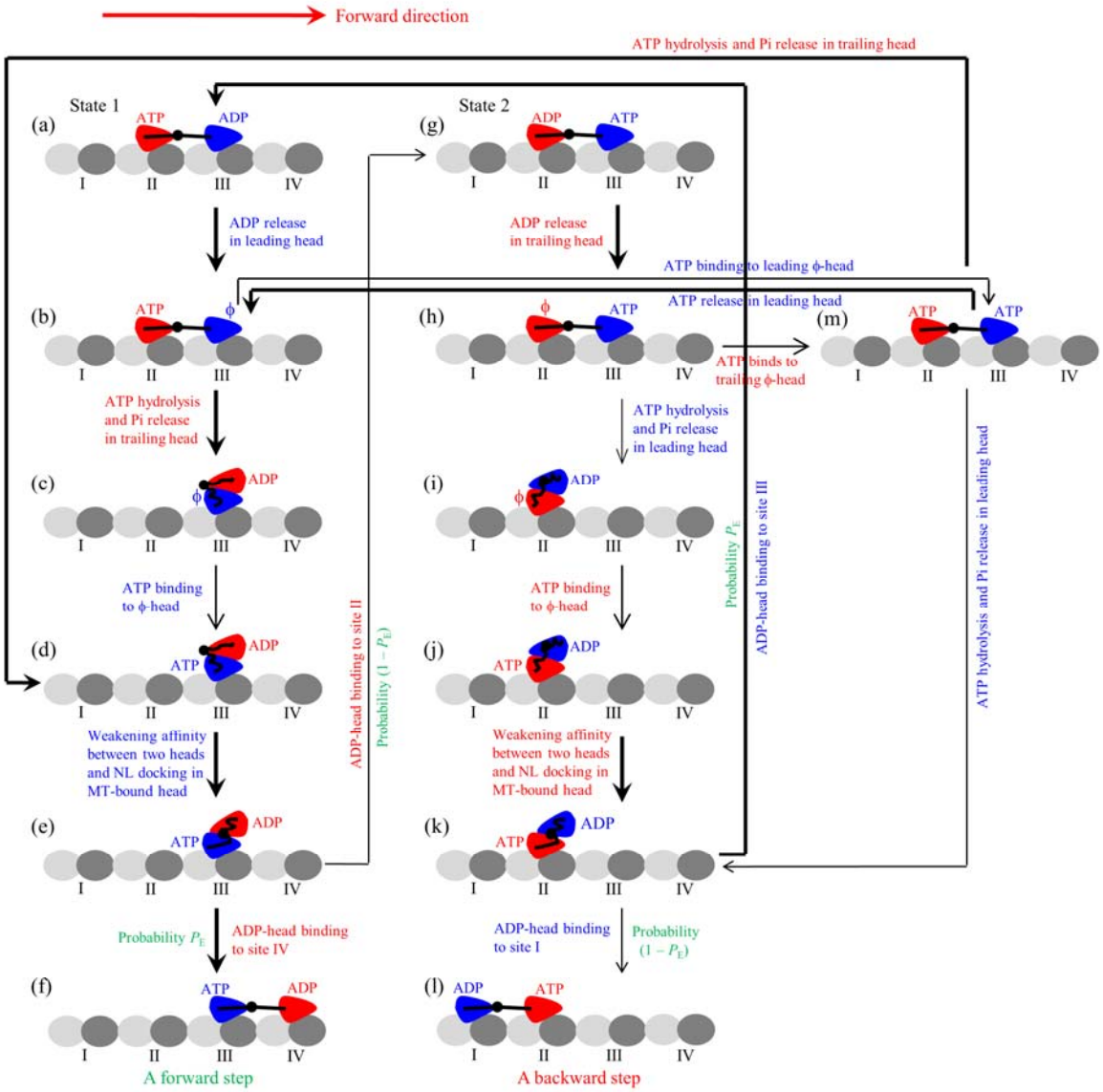

Figure S5. Schematic illustrations of kinesin stepping at low ATP concentrations. **(a) – (m)** The pathway of chemomechanical coupling. The thickness of the arrow represents the magnitude of the transition rate or probability under no load. The occurrences of Period I and Period II when the dimer has the weak binding energy to MT are not shown. For simplicity, ATP hydrolysis and Pi release are treated here as one step, with symbol ATP representing both ATP and ADP.Pi states, because in both ATP and ADP.Pi state the head binds strongly to MT. As a result, the change of ATP to ADP shown here consists of two sequential transitions including the transition of ATP to ADP.Pi and that of ADP.Pi to ADP.

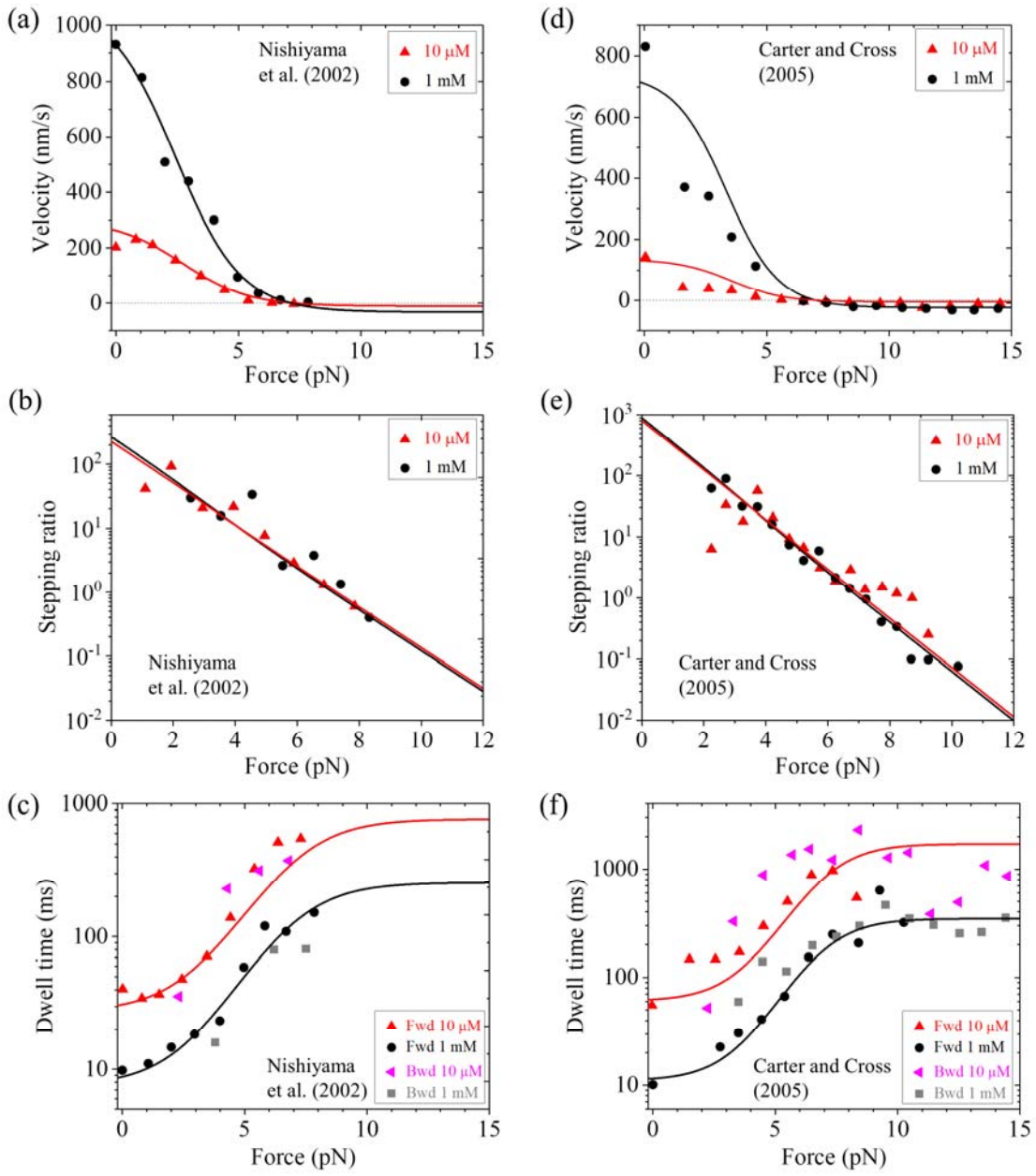

Figure S6. Results for bovine brain and *Drosophila* kinesin motors at different ATP concentrations. Lines are theoretical results. **(a – c)** Results for bovine brain kinesin, with the experimental data (symbols) taken from Nishiyama et al.[S9] (adapted by permission from Springer Nature). **(d – f)** Results for *Drosophila* kinesin, with the experimental data (symbols) taken from Carter and Cross[S8] (adapted by permission from Springer Nature).

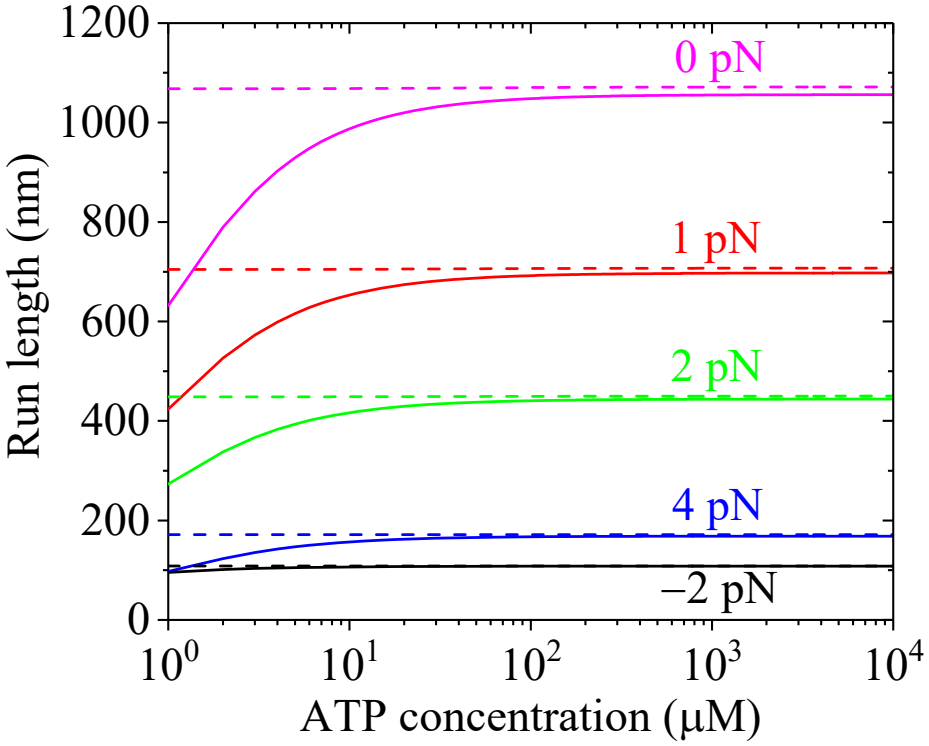

Figure S7. Theoretical results of run length versus ATP concentration for different values of *F*. Dashed lines correspond to the case that the dissociation can only occur in the weak MT-binding state, with $\varepsilon_{s0} = 0$. Solid lines correspond to the case that the dissociation can occur in both the weak and strong MT-binding states, with $\varepsilon_{s0} = 0.01\ s^{-1}$. The data are calculated using Eqs. (S1) – (S3), (S5) and (S24) – (S27), with parameter values given in Table S1 for *Drosophila* kinesin.

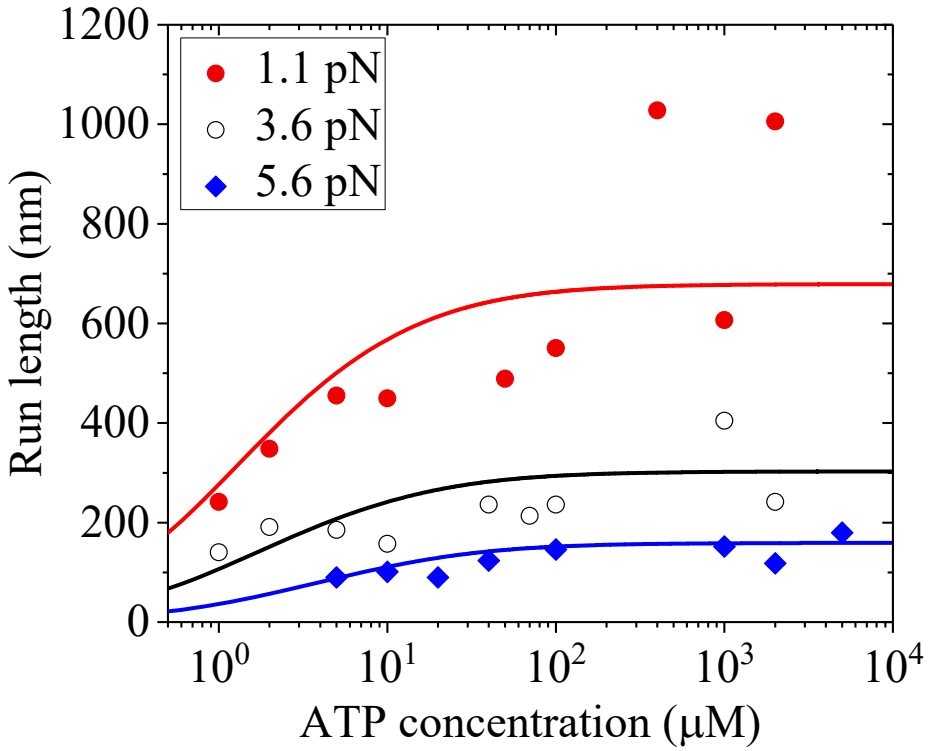

Figure S8. Results of run length versus ATP concentration under different values of F for squid optic lobe kinesin motor. Lines are theoretical data calculated by considering that the motor can dissociate in both the weak and strong MT-binding states, with parameter values given in Table 1, $k_b = 2\ \mu M^{-1}s^{-1}$, $k_{-1} = 10\ s^{-1}$ and $\varepsilon_{s0} = 0.02\ s^{-1}$. Symbols are experimental data taken from Schnitzer et al.[S12] (adapted by permission from Springer Nature).

Table S1. Parameter values for different species of kinesin.

Parameter	Bovine brain kinesin under condition of Nishiyama et al.[S9]	*Drosophila* kinesin under condition of Carter and Cross[S8]
$k^{(+)}$ (s^{-1})	136	95
$k^{(-)}$ (s^{-1})	4	3
E_{NL} (k_BT)	2.1	3.34
$d^{(+)}$ (nm)	3	3.8
k_D (s^{-1})	250	250
k_{NL} (s^{-1})	–	1500
k_{w0} (s^{-1})	–	5
δ_w (nm)	–	2.2
k_b ($\mu M^{-1}s^{-1}$)	5	2
k_{-1} (s^{-1})	100	80

Symbol "–" denotes that the value is not required in the calculation.

References

(S1) Xie, P.; Guo, S.-K.; Chen, H. ATP-concentration- and force-dependent chemomechanical coupling of kinesin molecular motors. *J. Chem. Inf. Model.* **2019**, *59*, 360−372.

(S2) Xie, P.; Guo, S.-K., Chen, H. A generalized kinetic model for coupling between stepping and ATP hydrolysis of kinesin molecular motors. *Int. J. Mol. Sci.* **2019**, *20*, 4911.

(S3) Shang, Z.; Zhou, K.; Xu, C.; Csencsits, R.; Cochran, J. C.; Sindelar, C. V. High-resolution structures of kinesin on microtubules provide a basis for nucleotide-gated force-generation. *eLife* **2014**, *3*, e04686.

(S4) Fehr, A. N.; Gutiérrez-Medina, B.; Asbury, C. L.; Block, S. M. On the origin of kinesin limping. *Biophys. J.* **2009**, *97*, 1663-1670.

(S5) Cao, L.; Wang, W.; Jiang, Q.; Wang, C.; Knossow, M.; Gigant, B. The structure of apo-kinesin bound to tubulin links the nucleotide cycle to movement. *Nature Comm.* **2014**, *5*, 5364.

(S6) Sindelar, C. V.; Downing, K. H. An atomic-level mechanism for activation of the kinesin molecular motors. *Proc. Natl. Acad. Sci. U.S.A.* **2010**, *107*, 4111–4116.

(S7) Shi, X.-X.; Guo, S.-K.; Wang, P.-Y.; Chen, H.; Xie, P. All-atom molecular dynamics simulations reveal how kinesin transits from one-head-bound to two-heads-bound state. *Proteins* **2020**, DOI: 10.1002/prot.25833.

(S8) Carter, N. J.; Cross, R. A. Mechanics of the kinesin step. *Nature* **2005**, *435*, 308−312.

(S9) Nishiyama, M.; Higuchi, H.; Yanagida, T. Chemomechanical coupling of the forward and backward steps of single kinesin molecules. *Nat. Cell Biol.* **2002**, *4*, 790−797.

(S10) Visscher, K.; Schnitzer, M. J.; Block, S. M. Single kinesin molecules studied with a molecular force clamp. *Nature* **1999**, *400*, 184-189.

(S11) Andreasson, J. O. L.; Milic, B.; Chen, G.-Y.; Guydosh, N. R.; Hancock, W. O.; Block, S. M. Examining kinesin processivity within a general gating framework. *eLife* **2015**, *4*, e07403.

(S12) Schnitzer, M. J.; Visscher, K.; Block, S. M. Force production by single kinesin motors. *Nat. Cell Biol.* **2000**, *2*, 718−723.